Radio Science, Volume 27, Number 5, Pages 593–610, September–October 1992

The propagation of mixed polarization VLF ($f \leq 5$ kHz) radio waves in the Antarctic Earth-ionosphere waveguide

P. D. Cotton[1]

Department of Physics, University of Sheffield, England

A. J. Smith

British Antarctic Survey, Cambridge, England

T. G. Wolf, W. L. Poulsen and D. L. Carpenter

STAR Laboratory, Stanford University, Stanford, California

(Received January 31, 1991; revised November 14, 1991; accepted February 20, 1992.)

During 1986, a series of special VLF transmissions at ~3 kHz and ~5 kHz were made from the crossed dipole antenna at Siple Station, Antarctica, which simulated transmissions from a single horizontal dipole at a number of different orientations. The subionospheric signals thus excited were recorded at four Antarctic stations: Faraday, Halley, South Pole and Arrival Heights (McMurdo Sound). The signals excited broadside to the dipole were seen to exhibit characteristics notably different from those of signals excited along the axis of the antenna, showing a minimum in received power (the depth of the minimum decreasing for the more highly attenuating paths) and increases in apparent arrival azimuth error and elevation angle. A simple computer model for mode propagation close to 5 kHz in the Antarctic Earth-ionosphere waveguide showed that these variations were the consequence of two effects: the preferential excitation of quasi-transverse magnetic (QTM) modes along the axis of the antenna and the lower attenuation of quasi-transverse electric (QTE) modes (with respect to QTM modes) over the Antarctic ice sheet. These results have important implications for studies involving the subionospheric propagation of signals with frequencies at the lower end of the VLF band and over highly attenuating surfaces, showing that QTE modes play a significant and sometimes dominant role. The propagation characteristics derived from the model may be applied to studies of the effect of burst energetic electron precipitation on subionospheric VLF signals (the Trimpi effect). Furthermore, the mode structure of subionospheric VLF signals radiated from the Siple transmitter, or a similar facility in Antarctica, may be controlled through the appropriate choice of signal frequency and antenna arrangement.

[1]Now at James Rennell Centre for Ocean Circulation, Southampton, England

Paper number 92RS00908.
0084-6604/92/92RS-00908$08.00

INTRODUCTION

There is a vast literature on the subject of VLF radio wave propagation. However, the problem appropriate to the Siple experimental VLF transmitter in Antarctica [*Helliwell and Katsufrakis*, 1978], namely, the excitation of signals at the low end of the VLF range (3 kHz

$\leq f \leq$ 10 kHz) from a long horizontal dipole antenna situated on a thick, poorly conducting ice sheet, and their subsequent propagation between a variable high-latitude ionosphere and an ice sheet of spatially varying thickness, has been less extensively studied. This paper reports an experiment to investigate the problem, using a crossed dipole transmitting antenna arrangement at Siple and a network of Antarctic receiving stations and describes a simple computer model for waveguide mode propagation which was developed to interpret the experimental data obtained. The main motivation for the work is the possible use of such a network for remotely detecting and mapping the burst precipitation of energetic particles into the lower ionosphere through the resulting perturbation of subionospherically propagating signals (the Trimpi effect [e.g., *Inan and Carpenter*, 1987]). The region spanned by the network is linked by geomagnetic field lines to regions of great geophysical complexity, for example, the plasmapause, auroral zone and polar cusp, where observations of such phenomena may be an important technique for understanding precipitation processes. The application of the model to the Trimpi phenomenon, and comparison with observations (e.g., by *Carpenter et al.* [1985]) has been reported in a second paper [*Cotton and Smith*, 1991]. We begin by reviewing some previous work relevant to VLF propagation in Antarctica.

The principal characteristic of VLF propagation over thick ($\gtrsim$1 km) ice, typical of the interior of Antarctica or Greenland, is the high attenuation rate compared with propagation over sea or ice-free land [*Webber and Peden*, 1971; *Field et al.*, 1972]. *Dowden and Holzworth* [1988] have recently estimated daytime attenuation rates in excess of 20 dB Mm^{-1} at 5 kHz, from balloon observations of VLF hiss over Antarctica. One consequence of this is a diffraction effect around the ice-covered Antarctic continent, caused by the lower attenuation over sea [*Barr*, 1987; *Kelly et al.*, 1988]. Both *Webber and Peden* [1971] and *Westerlund and Reder* [1973] have noted that the presence of a thick, poorly conducting ice layer can result in unusual "Brewster modes" in which the ground reflection coefficient is a minimum and the attenuation rate is particularly high. These authors have also pointed out that QTE modes should be attenuated less over thick ice than QTM modes, though there has been little experimental evidence to confirm this. A further important consideration for subionospheric propagation over Antarctica is the variability of the ionosphere as a result of specifically high-latitude phenomena. Although VLF is generally less affected than, for example, HF, which suffers the well-known auroral blackout as a result of increased absorption in the D layer; nevertheless, propagation can be greatly affected by phenomena such as solar proton events, which produce ionization at low altitudes. *Kelly et al.* [1988] noted variations of up to 20 dB in nighttime VLF wave fields, equivalent to lowering of the reflection height by up to 7 km (see also *Kossey et al.* [1983]).

In an earlier study of signals transmitted from a single (east-west) horizontal dipole antenna at Siple and received at Palmer station, *Tkalcevic* [1983] reported large arrival-bearing errors, which were attributed to the horizontal polarization of signals excited broadside to the dipole. Although *Tkalcevic* used a ray theory treatment, his conclusion was equivalent to the dominance of QTE mode(s) at the receiver. He also noted that reception was highly sensitive to ionospheric variability. More recently, *Carpenter et al.* [1988] compared signals transmitted from a longer 42-km dipole at Siple and received at South Pole, Palmer and Halley stations, all approximately the same distance from the transmitter. On this occasion, signals at 2.5 kHz were weakly received at Halley but recorded more strongly at Palmer and South Pole. It was suggested that the weaker signals recorded at Halley were the result of the high attenuation of QTM modes (which were excited preferentially in the direction of Halley) at this frequency. The signals were thought to be stronger at South Pole and Palmer because QTE modes would be excited more strongly in these directions, and the lowest order QTE mode undergoes less attenuation over ice than its QTM equivalent at these frequencies. During the same series of transmissions an unexpectedly strong third harmonic component was recorded at Halley (but not at Palmer or South Pole). This reception at Halley only was attributed in part to the properties of the Siple antenna and to the orientation of the Siple–Halley great circle path with respect to the antenna radiation pattern.

In both the above studies, only a single fixed dipole transmitting antenna was available at Siple, and there was thus no capability for changing the effective dipole orientation, a unique feature of the experiment reported here. The map of Figure 1 shows the experimental arrangement, with the paths from the transmitter (Siple) to the four receivers, Halley, Faraday, South Pole and Arrival Heights (McMurdo Sound), traversing a variety of ground conditions (sea, thin shelf ice, thick ice over rock, or a mixture) and latitude ranges. We have used phased orthogonal dipoles at Siple to simulate a single horizontal dipole at a number of orientations and have thus been able to carry out a more comprehensive study of the excitation and propagation of VLF signals in the Antarctic Earth-ionosphere waveguide than has been attempted previously. In the next section we briefly describe the transmissions made during this waveguide experiment and the measurements made at the receiving sites. In later sections we develop a simple computer model for waveguide mode propagation, to aid in interpreting the data, and we report observations and compare them with the predictions of the model.

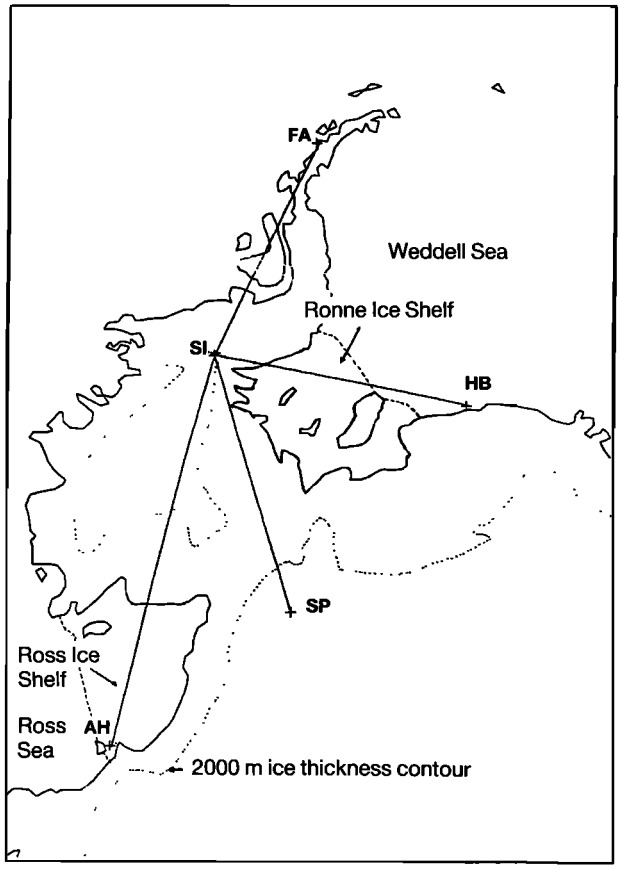

Fig. 1. Map of western Antarctica, indicating the position of the five stations involved in the waveguide probing experiment: Faraday (FA); Halley (HB); Siple (SI); South Pole (SP); and Arrival Heights (AH) (McMurdo Sound). The dotted line indicates the 2000-m ice thickness contour, and the dashed lines indicate the approximate edges of floating ice shelves.

THE 1986 WAVEGUIDE EXPERIMENT

Transmitter

Figure 2 shows the transmitting antenna configuration at Siple in 1986. The "short" (21.2 km) and "long" (42.4 km) magnetic east-west antennas described by *Carpenter et al.* [1988] had been supplemented by a second short (21.2 km) antenna, oriented north-south. By varying the relative powers and phases of the transmitter outputs to the two short dipoles, signals of any desired polarization could be produced. The main purpose of this was to increase the power of whistler mode waves injected into the magnetosphere, by transmitting signals of the correct polarization for whistler mode propagation (right-hand circularly polarized) [*Helliwell*, 1988]. In the waveguide experiment, eight different linear polarizations were transmitted, corresponding to dipole orientations differing by 22.5° (i.e., magnetic E-W, ESE-WNW, SE-NW, SSE-NNW, S-N, SSW-NNW, SW-NE, and WSW-ENE), plus left- and right-handed circular polarizations. For each polarization, the transmitter was configured for maximum possible output power, with the result that the actual power varied in the range 58–135 kW. All received signal powers shown here have been normalized to 135 kW.

Transmission format and experimental conditions

The operational plan was designed to provide data for different frequencies and ionospheric conditions. Each of the eight linear polarizations was transmitted for 3 min 30 s followed by a key up interval of 1 min 30 s. Then the two circular polarizations were each transmitted for 1 min 30 s, again followed by a gap of 1 min 30 s. The entire 44 min 30 s-long sequence was transmitted beginning at 0800 UT each day during June 23–27, and July 23–25, 1986, and beginning at 1700 UT each day during September 15–19 and 22–26, 1986. Transmissions were made at 4.98 kHz and 3.00 kHz on alternate days. For the June and July transmissions, all propagation paths were entirely in darkness, and geomagnetically quiet conditions prevailed (maximum $Kp = 2$). In September, propagation to Faraday, Halley, and South Pole was under a sunlit ionosphere; conditions were also more disturbed ($Kp \leq 5$).

Receiving systems

The receivers at Halley and Faraday were crossed loop VLF broadband goniometer systems, with record-

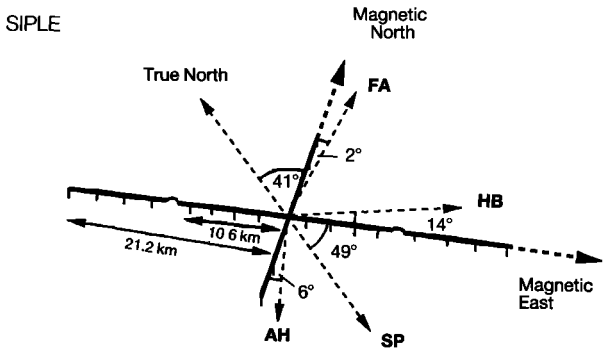

Fig. 2. The layout of the VLF transmitting antennas at Siple Station. The directions of the great circle paths to Faraday, Halley, South Pole and Arrival Heights are indicated (based on a figure from *Carpenter et al.* [1988]).

ing to analogue magnetic tape [*Bullough and Sagredo,* 1973]. At Arrival Heights and South Pole, broadband nondirection-finding receivers were used. At Arrival Heights, crossed loops were also used, so that, as at Halley and Faraday, received horizontal power measurements were independent of polarization. In contrast, the South Pole receiver was connected to a single loop, oriented magnetically north-south, making it more sensitive to QTM modes from Siple than QTE modes. In addition, a digital signal processor (DSP), part of the Advanced VLF Data Analysis System (AVDAS) [*Smith and Yearby,* 1987] was operated at Halley. In the DSP, signals received by the two crossed loops and also by a vertical electric field antenna were digitally sampled and recorded.

The receiving loop antennas at Halley and Faraday were oriented in the (geographic) north-south and east-west vertical planes and were thus sensitive to the H_X and H_Y components of the wave magnetic field, respectively. For convenience we use a right-handed coordinate system fixed relative to the receiver, in which the X is eastward, Y is northward and Z is upward; it is related by a rotation about the Z axis to the (x, y, z) system used in the waveguide propagation model, in which the x axis points along the propagation direction (Figure 3). In the goniometer, the signals received by the loops are combined as follows to give the rms wave magnetic field amplitude H corresponding to the horizontal power flux ($c\mu_0 H^2$), and the apparent arrival azimuth ψ (measured clockwise from geographic north).

$$H = \left(\frac{|H_X|^2 + |H_Y|^2}{2}\right)^{1/2} \tag{1}$$

$$\psi = \frac{1}{2}\tan^{-1}\left(\frac{-2\Re(H_X H_Y^*)}{|H_X|^2 - |H_Y|^2}\right) \tag{2}$$

The goniometer gives the correct azimuth for a vertically polarized, horizontally propagating plane wave but may otherwise be subject to polarization and multipath errors [*Bullough and Sagredo,* 1973; *Tsuruda and Ikeda,* 1979; *Strangeways,* 1980]. There is a 180° ambiguity.

In the DSP system, H_X, H_Y and E_Z are digitized in real time. The power is still computed from (1), but the arrival azimuth can now be computed from the equation

$$\psi = \arctan\left\{\frac{\Re(E_Z H_X^*)}{\Re(E_Z H_Y^*)}\right\} \tag{3}$$

This expression not only resolves the 180° ambiguity of the goniometer but is in many cases less in error than (2) (except for example when the wave is nearly horizontally polarized so that E_Z is small). The DSP system also provides estimates of elevation angle β and ellipticity of polarization η through the expressions

$$\beta = \cos^{-1}\left\{\frac{\left[(\Re(E_Z H_X^*))^2 + (\Re(E_Z H_Y^*))^2\right]^{1/2}}{Z_0(|H_X|^2 + |H_Y|^2)}\right\} \tag{4}$$

$$\eta = \frac{-2\Im(H_X H_Y^*)}{|H_X|^2 + |H_Y|^2} \tag{5}$$

Equations (3)–(5) assume a single, plane elliptically polarized wave. Polarization η is defined so as to be +1 for right and −1 for left circular polarization (of the horizontal projection of the wave magnetic field), and zero for linear polarization. $\Re$ and $\Im$ denote the real and imaginary parts of a complex quantity. Z_0 is the characteristic impedance of free space ($\equiv (\mu_0/\epsilon_0)^{1/2}$).

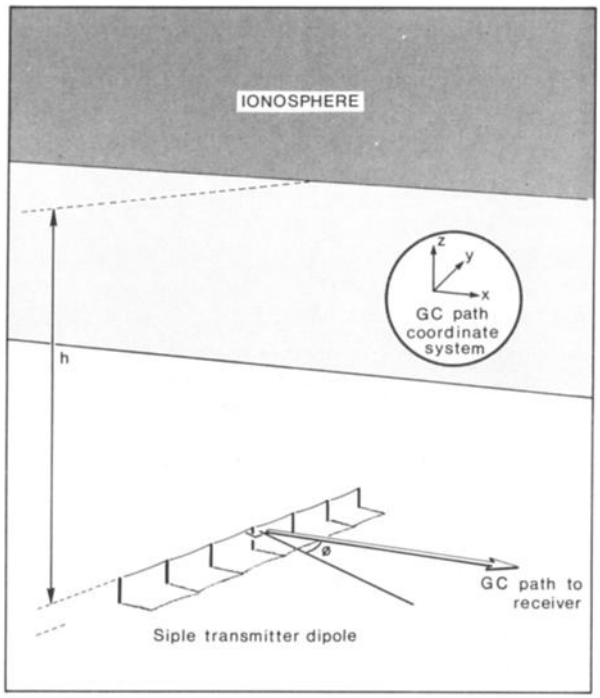

Fig. 3. The transmitter to receiver great circle path (TRGCP) coordinate system, as employed by the computer propagation model. The x axis is horizontal and lies along the direction of the TRGCP, y is horizontal and perpendicular to x, and z is vertical (positive upward). The variable h is the height of the Earth-ionosphere waveguide, ϕ is the angle between the TRGCP and the normal to the axis of the dipole, measured counterclockwise. The receiver coordinate system (X, Y, and Z) is related to the TRGCP system by a rotation around the z axis.

COMPUTER MODEL FOR WAVEGUIDE PROPAGATION

Background

An accurate, but adaptable, computer model for the propagation of VLF signals in the Antarctic Earth-ionosphere waveguide was required to assist in the interpretation of the data produced during the experiment described above. This model would be required to provide details of the mode structure of the propagating signal (i.e., strengths and polarizations of the dominant modes) so that the variations in signal characteristics (power, ellipticity, arrival azimuth and elevation), recorded at the four receiver sites could be correctly interpreted. It had to be capable of simulating the subionospheric propagation of signals at very low frequencies ($\leq$ 5 kHz), over a range of ionospheric conditions (night/day, quiet/disturbed), for signals excited at different orientations (ϕ) with respect to the transmitting dipole. To enable the model to calculate values for power, ellipticity, azimuth and elevation, at least three field components, H_x, H_y, and E_z (in the coordinate system for propagation) must be available.

It was determined that a mode theory model would be most appropriate in this application, as the low frequencies and path lengths of $\geq$ 1500 km would limit the number of modes required for the calculations. *Tkalcevic* [1983], in a study of propagation of 5-kHz signals from Siple to Palmer, found that 15 rays were required to provide an accurate representation. We shall see later that a model using no more than four modes provides a reasonably accurate mode theory representation of a similiar problem.

A number of sophisticated Earth-ionosphere waveguide propagation models have been used in previous studies, with the model developed at the Naval Ocean Systems Center, San Diego, California (the Long Wave Propagation Capability (LWPC) model) and employed by *Pappert and Ferguson* [1986] and *Tolstoy et al.* [1986] perhaps being the most thoroughly documented. However, in view of the unusual characteristics of the situation to be modeled (as outlined above) and of the fact that a diagnostic tool rather than a "black box" model was required, it was decided that the intentions of this study would be best served by a new propagation model. This model was designed to retain some of the capablilities of the LWPC model, whilst taking advantage of some approximations made possible by the high latitudes, low frequencies and relatively short path lengths pertaining in this case. It is important to note at this point that the model does not (and was not designed to) provide an exhaustively accurate simulation of VLF propagation in the Antarctic Earth-ionosphere waveguide. The rather basic model from which results are presented here was primarily designed to act as an aid in the interpretation of the experimental data.

Table 1 lists the approximations that were employed by the computer model used in this study and the limitations imposed as a result. A justification for these approximations may be found in large part in the work of *Barr* [1971*a*, *b*], who used a flat Earth approximation in studies of the propagation of VLF signals with frequencies less than 10 kHz. Although the effect of Earth curvature can still be significant at 10 kHz, the flat Earth approximation becomes more accurate as the signal frequency decreases further. *Barr* [1971*b*] also showed that a nonvertical magnetic field had a small and decreasing effect at magnetic latitudes greater than 60°. Later experimental work by *Barr* [1982] further showed that a "best fit" to VLF reflection data (for signals with frequencies of 7–8 kHz) was provided by an ionospheric model with a homogeneous density profile and a sharp cutoff at 88 km altitude.

The final approximation, that the model only considers propagation along the great circle (GC) propagation path joining the transmitter and receiver, is a consequence of the assumption that the waveguide is infinite and nonvarying in the horizontal direction perpendicular to propagation (the y direction).

The model employs a coordinate system as defined in Figure 3. Coordinates x, y and z are a right-handed set, with x defining the horizontal direction of propagation along the great circle path. The angle ϕ is that which the direction of the great circle path makes to the normal to the dipole axis, so that $\phi = \pm 90°$ represents excitation along the axis of the dipole, and $\phi = 0°$ represents excitation broadside to the dipole; z_0 is the height of the transmitting antenna above the ground (which is defined to be at $z = 0$); and h is the VLF reflection height.

Ground and ionosphere models

A two-layer model was adopted for the ground surface of the Antarctic. This assumed a layer of ice lying over

TABLE 1. Approximations in the VLF Waveguide Propagation Model for High Latitudes

Assumptions	Applicability/ Limitations
Sharply bounded homogeneous ionosphere	$f < 10$ kHz
Flat Earth	$f < 10$ kHz; path length < 2000 km
Vertical magnetic field	latitude $> 60°$
Great circle propagation only	no refraction or echoes

the (infinitely deep) lower surface of either wet rock or sea water. The frequency-dependent electrical properties for ice were derived from *Peden et al.* [1972]. This model for the bulk properties of the ice sheet, though not explicitly temperature- dependent, was shown by *Raghuram et al.* [1974] to agree well with values derived for a five-layer ice model which included realistic ice temperatures. It is known that the ice temperature is an important consideration affecting waveguide propagation over deep polar ice caps [*Kelly and Byrd*, 1989]. However, the complexity of the topography of the Antarctic ice sheets over the wide geographical regions discussed here, put a meaningful discussion of such effects beyond the scope of this paper.

The electrical properties for the various ground surfaces (as used by the model) are given in Table 2. Fresnel reflection coefficients for the ground surface may be calculated for the case of incident waves exhibiting two polarizations. ${}_{\parallel}\bar{R}_{\parallel}$ represents the coefficient for the reflection of a transverse magnetic (TM) wave, which contains the field components H_y (hence TM), E_x and E_z; and the coefficient ${}_{\perp}\bar{R}_{\perp}$ represents the reflection of a transverse electric (TE) wave, containing the components H_x, H_z and E_y. In this context, the subscripts $\parallel$ and $\perp$ historically (though perhaps confusingly) refer to the polarization of the electric vector of the incident (first subscript) or reflected (second subscript) wave, with regard to the plane of incidence at waveguide boundary. This plane of incidence in our presently defined coordinate set is the x-z plane. These coefficients are functions of the ground conductivity and permittivity, and of the mode angle θ, and are usually represented in matrix form as

$$[R_g] = \begin{bmatrix} {}_{\parallel}\bar{R}_{\parallel} & 0 \\ 0 & {}_{\perp}\bar{R}_{\perp} \end{bmatrix} \tag{6}$$

Table 3 lists the different ionospheric parameters used by the model. Initial modeling employed the values used by *Webber and Peden* [1971] for polar nighttime conditions (i.e., h, ionospheric reflection height, which is 85 km; ν, collision frequency, which is 10^6 Hz; and N, electron density, which is 2×10^8 el m^{-3}). However, subsequent modeling and reference to the work of *Kossey et al.* [1983] indicated that the higher reflection heights and lower collision frequencies were more appropriate. The ionospheric reflection coefficients are usually represented as

$$[R_i] = \begin{bmatrix} {}_{\parallel}R_{\parallel} & {}_{\parallel}R_{\perp} \\ {}_{\perp}R_{\parallel} & {}_{\perp}R_{\perp} \end{bmatrix} \tag{7}$$

These coefficients may be derived from the parameters h, ν, N, and f (signal frequency) and mode angle θ through expressions used by *Wait and Perry* [1957]. The ionosphere is a magnetized plasma, so a wave incident on the ionosphere will undergo a partial change of polarization on reflection, as represented by the elements, ${}_{\parallel}R_{\perp}$ and ${}_{\perp}R_{\parallel}$. The presence of these elements causes mixing between the two mode polarizations TE and TM, resulting in two less distinct mode series labeled QTE and QTM.

TABLE 2. Electrical Properties of Various Types of Antarctic Terrain, as Used in the Propagation Model

Surface Description	Relative Permittivity, ε_r	Conductivity, σ, mhos m^{-1}	Source
	Bulk Properties of Ice Sheet (Frequency Dependent)		
Ice (5.0 kHz)	26.5	1.02×10^{-5}	*Peden et al.* [1972]
Ice (3.0 kHz)	46.0	6.7×10^{-6}	
	Other Surfaces (Frequency Independent)		
Ocean water	81.0	5.0	*Harth* [1982]
Mountainous rock	1.0	1.0×10^{-4}	
Wet continental rock subsurface	10.0	1.0×10^{-3}	

TABLE 3. Ionospheric Parameters Used in Modeling the Results of the 1986 Antarctic Waveguide Probing Experiment

Model	VLF Reflection Height, km	Electron Density, el m^{-3}	Collision Frequency, MHz	Gyro Frequency, MHz
		High Latitude, HB, SP, AH		
Night (quiet)	92.0	2.0×10^8	0.85	1.6
Day (quiet)	82.0	2.0×10^8	0.85	1.6
Day (disturbed)	80.0	2.0×10^8	0.85	1.6
		Mid-Latitude, FA		
Night (quiet)	92.0	2.0×10^8	0.85	1.2
Day (quiet)	82.0	2.0×10^8	0.85	1.2
Day (disturbed)	80.0	2.0×10^8	0.85	1.2

The ground and ionospheric reflection coefficients are combined in the waveguide resonance condition known as the mode equation, here presented for a flat Earth:

$$\{{}_{\parallel}R_{\parallel}\ {}_{\parallel}\bar{R}_{\parallel} - e^{2\imath(kh\cos\theta - n\pi)}\} \cdot \{{}_{\perp}R_{\perp}\ {}_{\perp}\bar{R}_{\perp} - e^{2\imath(kh\cos\theta - n\pi)}\} - ({}_{\parallel}R_{\perp}\ {}_{\parallel}\bar{R}_{\parallel})\,({}_{\perp}R_{\parallel}\ {}_{\perp}\bar{R}_{\perp}) = 0 \quad (8)$$

where k is the free space wave number, h is the reflection height of the waveguide, and n is a nonnegative integer running from 0 to ∞.

The solutions to (8) form two infinite sets, the QTM and the QTE modes. Because the reflection coefficients are themselves dependent on the mode angle, the mode equation must be solved iteratively, using an estimate for θ as the initial input. Solutions for the situations modeled in this paper were achieved by solving (8) in the limit of perfectly conducting waveguide walls and then applying more realistic conditions step by step. To act as a check on this method, a recently obtained version of the mode-finding program, MODESRCH [*Morfitt and Shellman*, 1976] was used to search the complex plane for solutions to the mode equation (8). Using the same ground and ionosphere parameters, the search revealed that each method produced the same modes, with essentially the same properties. The mode numbering was also initialized at the perfect conductivity limit (in order of increasing attenuation), and continuity in numbering maintained to the modeled conditions of the waveguide, a system suggested by *Wait* [1962]. In some later figures, lower-order modes may exhibit a higher attenuation rate than one or more higher-order modes, contrary to usual expectation. Note that the mode numbers used here are independent of mode type, and that all modes (QTM and QTE) are included in one numbering system.

Field component expressions

General expressions giving the six field components at any location within the waveguide are derived by solving the waveguide boundary conditions for generalized wave functions which contain the solution for a horizontal dipole source. The resulting expressions for H_x, H_y and E_z are sums over the mode series ($m = 1, \ldots, M$, including both QTE and QTM modes) and are given in (9) to (11):

$$H_x = \frac{\pi \mathcal{M} k^3}{Z_0} \sum_m \Lambda_E^m h_x^m(z) \mathrm{H}_0^2(kS^m x) \quad (9)$$

$$H_y = \frac{\pi \mathcal{M} k^3}{Z_0} \sum_m \Lambda_M^m h_y^m(z) \mathrm{H}_0^2(kS^m x) \quad (10)$$

$$E_z = -\pi \mathcal{M} k^3 \sum_m \Lambda_M^m e_z^m(z) \mathrm{H}_1^2(kS^m x) \quad (11)$$

where $\mathcal{M}$ is the antenna propagation factor and is given by

$$\mathcal{M} = \frac{I_0 dS}{4\imath k} Z_0 \quad (12)$$

I_0 is the effective antenna current, and dS the dipole length, so that $I_0 dS$ is the dipole moment. Λ_M and Λ_E are the QTM and QTE excitation functions, dependent only on waveguide conditions close to the transmitting antenna, and are given by

$$\Lambda_M = \left[\left(\frac{\frac{1}{\imath k} f_h'(z_0)\,(e^{2\imath kCh} - {}_{\perp}\bar{R}_{\perp}\ {}_{\perp}R_{\perp})}{{}_{\parallel}\bar{R}_{\parallel}}\right)\cos\phi + ({}_{\perp}R_{\parallel}\ f_e(z_0)\sin\phi)\right] \frac{(1 + {}_{\parallel}\bar{R}_{\parallel})\,e^{2\imath Ckh}}{d\Delta/dC} \quad (13)$$

$$\Lambda_E = \left[\left(\frac{f_e(z_0)\,(e^{2\imath kCh} - {}_{\parallel}\bar{R}_{\parallel}\ {}_{\parallel}R_{\parallel})}{{}_{\perp}\bar{R}_{\perp}}\right)\sin\phi + \left(\frac{1}{\imath k}\,{}_{\parallel}R_{\perp}\ f_h'(z_0)\cos\phi\right)\right] \cdot \frac{(1 + {}_{\perp}\bar{R}_{\perp})\,e^{2\imath Ckh}}{Z_{eh}\,d\Delta/dC} \quad (14)$$

$f_h(z)$ and $f_e(z)$ are QTM and QTE height gain functions and the prime (e.g., f_e') indicates the differential of the function with respect to z.

$$f_h(z) = e^{\imath kCz} + {}_{\parallel}\bar{R}_{\parallel}\ e^{-\imath kCz} \quad (15)$$

$$f_e(z) = e^{\imath kCz} + {}_{\perp}\bar{R}_{\perp}\ e^{-\imath kCz} \quad (16)$$

Z_{eh} is the coupling impedance:

$$Z_{eh} = \frac{(1 + {}_{\perp}\bar{R}_{\perp})\,(e^{2\imath kCh} - {}_{\parallel}\bar{R}_{\parallel}\ {}_{\parallel}R_{\parallel})}{(1 + {}_{\parallel}\bar{R}_{\parallel})\ {}_{\perp}R_{\parallel}\ {}_{\perp}\bar{R}_{\perp}} = \frac{(1 + {}_{\perp}\bar{R}_{\perp})\ {}_{\parallel}R_{\perp}\ {}_{\parallel}\bar{R}_{\parallel}}{(1 + {}_{\parallel}\bar{R}_{\parallel})\,(e^{2\imath kCh} - {}_{\perp}\bar{R}_{\perp}\ {}_{\perp}R_{\perp})} \quad (17)$$

The function Δ is given by

$$\Delta = \begin{vmatrix} {}_{\perp}\bar{R}_{\perp}\ {}_{\perp}R_{\parallel} & {}_{\perp}\bar{R}_{\perp}\ {}_{\perp}R_{\perp} - e^{2\imath kCh} \\ {}_{\parallel}\bar{R}_{\parallel}\ {}_{\parallel}R_{\parallel} - e^{2\imath kCh} & {}_{\parallel}\bar{R}_{\parallel}\ {}_{\parallel}R_{\perp} \end{vmatrix} \quad (18)$$

Finally, $h_x(z)$, $h_y(z)$ and $e_z(z)$ are normalized height gain functions:

$$h_x(z) = \frac{\frac{1}{\imath k} f_e'(z)}{1 + {}_{\perp}\bar{R}_{\perp}} Z_{eh} \quad (19)$$

$$h_y(z) = \frac{f_h(z)}{1 + {}_{\parallel}\bar{R}_{\parallel}} \quad (20)$$

$$e_z(z) = \frac{-\imath S f_h(z)}{1 + {}_{\|}\bar{R}_{\|}} \tag{21}$$

S is the mode sine, C is the mode cosine, and k, ϕ, h, z, and z_0 are as previously defined. $H_0^2(kSx)$ and $H_1^2(kSx)$ are Hankel functions of the second kind, 0th and first order, with arguments kSx [*Watson*, 1922].

The equations (9) to (21) hold for a waveguide with uniform boundary parameters and can be shown to be consistent with those used by *Webber and Peden* [1971] and to be flat Earth equivalents of expressions used by *Pappert and Ferguson* [1986]. The full Hankel functions were employed, rather than their exponential approximations ($e^{\imath kSx}$), because the model was to be used to study variations of field over short distances, where the exponential approximation becomes inaccurate.

The field component expressions (9) to (11) were then modified to permit changes in waveguide parameters. At any boundary between different sets of waveguide parameters, a new set of waveguide modes are excited, and the efficiency with which each member (n) of the new set of modes is excited by each of the original set of modes (m) is determined by the transmission coefficient TC_{mn}. These transmission coefficients are obtained by matching tangential field component functions from an incident mode, across the boundary to the new set of waveguide parameters, with the equivalent functions of the whole set of new waveguide modes ($n = 1, \ldots, N$), and then integrating up the height of the waveguide. This procedure results in the formation of a set of M ($m = 1, \ldots, M$) simultaneous equations which may be solved for the TC_{mn} (see for example, *Galejs* [1972] and *Pappert and Snyder* [1972]).

Any field component of the mode n in the second section is calculated from the incident field components at the position of the boundary ($x = x_1$ and $z = 0$), divided by the relevant height gain function, multiplied by the transmission coefficients, and summed over the original mode series. This is then multiplied by the height gain functions and Hankel functions for the new waveguide section (effective from x_1). Equation (22) gives an example of this calculation for the H_x field component of mode n:

$$H_x = \left(\sum_m \frac{TC_{mn} H^m_{x(x=x_1,z=0)}}{h^m_x(0)} \right) h^n_x(z) \frac{H_0^2(kS^n x)}{H_0^2(kS^n x_1)} \tag{22}$$

To calculate the field components along a given GC propagation path, the path was first separated into a number of waveguide sections within each of which the waveguide parameters were set constant. The mode equation would then be solved for all the significant modes in each section, and the mode angles and waveguide parameters then input to the main program. This program could output values for individual mode field parameters and derived signal characteristics for the total signal (e.g., received power, ellipticity, arrival azimuth, elevation, calculated for the appropriate receiving antenna configuration), for any point on the great circle path.

Modeled propagation characteristics

Before signal variations along specific great circle paths are discussed, some general propagation characteristics for VLF waves excited in the Antarctic Earth-ionosphere waveguide, from which the specific variations are obtained, will be introduced.

It is well established that the thick, poorly conducting, ice caps of polar continental regions induce high attenuation and unusual propagation characteristics on subionospheric VLF signals. This anomalous behaviour comprises ambiguity in mode numbering (caused by apparent exchanges of propagation properties between modes) and the exhibition, in certain circumstances, of a form of the "Brewster" effect. This effect is seen only on QTM modes and is evident as a minimum in the ground reflection coefficient ${}_{\|}R_{\|}$. Consequently, this results in a maximum in the attenuation rate of the mode affected. *Westerlund and Reder* [1973] illustrated in a theoretical and experimental study that either of the two QTM modes that were considered could exhibit this form of the Brewster effect and that the exact details of this behaviour were dependent on the ice thickness, the signal frequency, and the ionospheric reflection height. It is not within the scope of this paper to include a full evaluation of this effect, but it is as well that the reader is aware of these unusual propagation properties.

Webber and Peden [1971] and *Pappert* [1970] showed that a horizontal dipole would excite VLF modes asymmetrically in the Earth-ionosphere waveguide. Calculations by our computer model, for 5-kHz signals excited by a 21.4-km horizontal dipole suspended over 2-km thick ice, under a night ionosphere, showed that broadside to the dipole ($\phi = 0°$) QTM and QTE modes of equal order would be excited at roughly similar strengths, (−46 dB and −40 dB, respectively, for the lowest-order QTM and QTE modes, numbers 1 and 2, dB with respect to an arbitrary reference value). However, in the axial or endfire direction ($\phi = \pm 90°$), QTM modes would be excited with ~20 dB greater power than the equivalent QTE mode (−25 dB and −46dB, respectively, for modes 1 and 2).

Figure 4 illustrates the variation in attenuation rates (calculated by our computer model) for a 5-kHz signal, under a nighttime ionosphere, with the thickness of the underlying ice sheet. This figure includes four modes, labeled 1–4. Modes 1 and 3 are QTM modes, and modes 2 and 4 are QTE modes. The 0th order

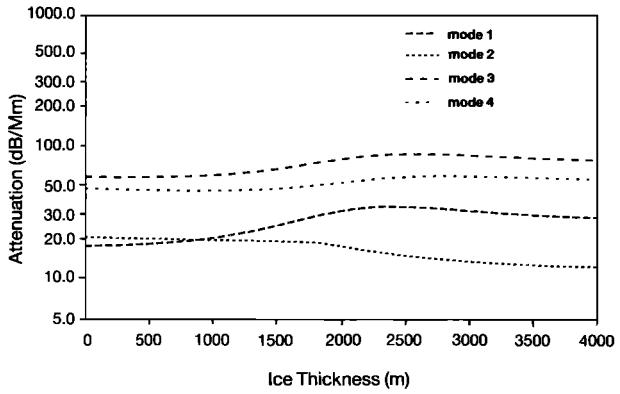

Fig. 4. The variation of attenuation rate with ice thickness, with an underlying surface of wet rock, for the four lowest-order modes of a 5-kHz signal propagating under a nighttime high-latitude ionosphere (Table 3). Modes 1 and 3 are QTM; modes 2 and 4 are QTE.

QTM mode, TM0 (sometimes referred to as the TEM mode), is not included in the calculations presented in this paper because it is not launched into the waveguide by a horizontal dipole [*Galejs*, 1972, p. 99].

Note that the QTM modes (1 and 3) are more strongly affected by the variation in ice thickness than are the QTE modes (2 and 4). Modes 1 and 3 appear to exhibit maxima in attenuation rates at ice thicknesses close to 2500 m, possibly examples of a form of the Brewster effect discussed above. The absolute values for the modeled attenuation rates were found to be highly sensitive to small variations in the ionospheric parameters, though the form of the variations with ice thickness (Figure 4) remained consistent. This result is a consequence of the use of a sharply bounded ionospheric model, and it is probable that this problem would not occur with the selection of a more realistic, exponentially decaying, ionospheric density model. However, for the reasons outlined previously, we decided to persist with the simpler model.

Depending on the thickness of the ice, nighttime attenuation rates of ~18–33 dB Mm^{-1} and daytime rates of 25- -40 dB Mm^{-1} (not illustrated) were calculated for the lowest-order QTM mode (1) of a 5-kHz signal. The daytime values appeared to be slightly high when compared with the theoretical value of 24 dB Mm^{-1} derived by *Field et al.* [1972], and the 22 ±6 dB Mm^{-1} obtained experimentally by *Dowden and Holzworth* [1988]. However, the models used to calculate these values were maintained, as they were subsequently found to produce accurate representations of the data recorded during the waveguide probing experiment.

Figure 5 illustrates modeled variations in mode powers and polarization ratios (p) for a signal propagating along the Siple–Arrival Heights GC propagation path (the longest path, and the one with the greatest part over deep ice, Figure 1). The segmentation for each propagation path was chosen so that there were no steps in ice thickness greater than 200 m between adjacent waveguide sections, and a new section was started at every transition from land or ice to sea. The original ice thickness model was obtained from *Drewry* [1983]. The polarization ratios are calculated from the ratio of the magnitudes of the H_x and H_y field components, as follows:

$$p = \frac{|H_x|}{|H_y|} \tag{23}$$

This ratio gives a measure of the QTM or QTE nature of a mode (or total signal), in that H_x is a component of a TE field and H_y a component of a TM field. Thus for $p > 1$, modes (or signals) are QTE polarized, and for $p < 1$, modes are QTM polarized. The further this ratio departs from unity, the "purer" the nature of the mode.

The left-hand panels of Figure 5 illustrate the variations in the signal excited in the endfire direction ($\phi = \pm 90°$). The QTM modes 1 and 3 ($p < 1$ in the middle left-hand panel) are excited most strongly, but the lowest-order QTE mode (mode 2, $p > 1$) undergoes less attenuation over the thick ice covering the early part of the GC path (bottom center panel). At 1500 km the strengths of modes 1 and 2 are similar, and these two modes are attenuated by similar amounts thereafter (as the GC path crosses the Ross ice shelf). These two modes have different phase velocities and so periodically move in and out of phase with each other, causing maxima and minima in the total signal strength. Note that the polarization ratio of the complete signal, p_{total}, rises from less than 1 at the start of the path, and then oscillates around a value close to 1 between 1500 km and 2500 km, indicating that this signal then has a mixed polarization.

On the broadside signal ($\phi = 0°$, right-hand panels), all modes 1–4 are excited at similar strengths, but the lower attenuation of mode 2 over the first section of the path results in this mode being dominant at Arrival Heights (by ~30 dB). The value of p_{total} initially shows some variation and then stays relatively constant at ~2, close to that of mode 2, after 1000 km. The difference in total signal strength between the broadside and axial signals (at Arrival Heights) is $\leq$ 6 dB, equal to the difference in the initial excitation factors of mode 2 at the two orientations (−40 dB at $\phi = \pm 90°$ and −46 dB at $\phi = 0°$), with the axial signal showing some extra contribution from mode 1 (maximum 6 dB, if mode 1 is of equal strength as mode 2).

The GC propagation path from Siple to Halley has a much shorter section over the deep ice sheet, and the two lowest-order modes, 1 and 2, undergo a similar total

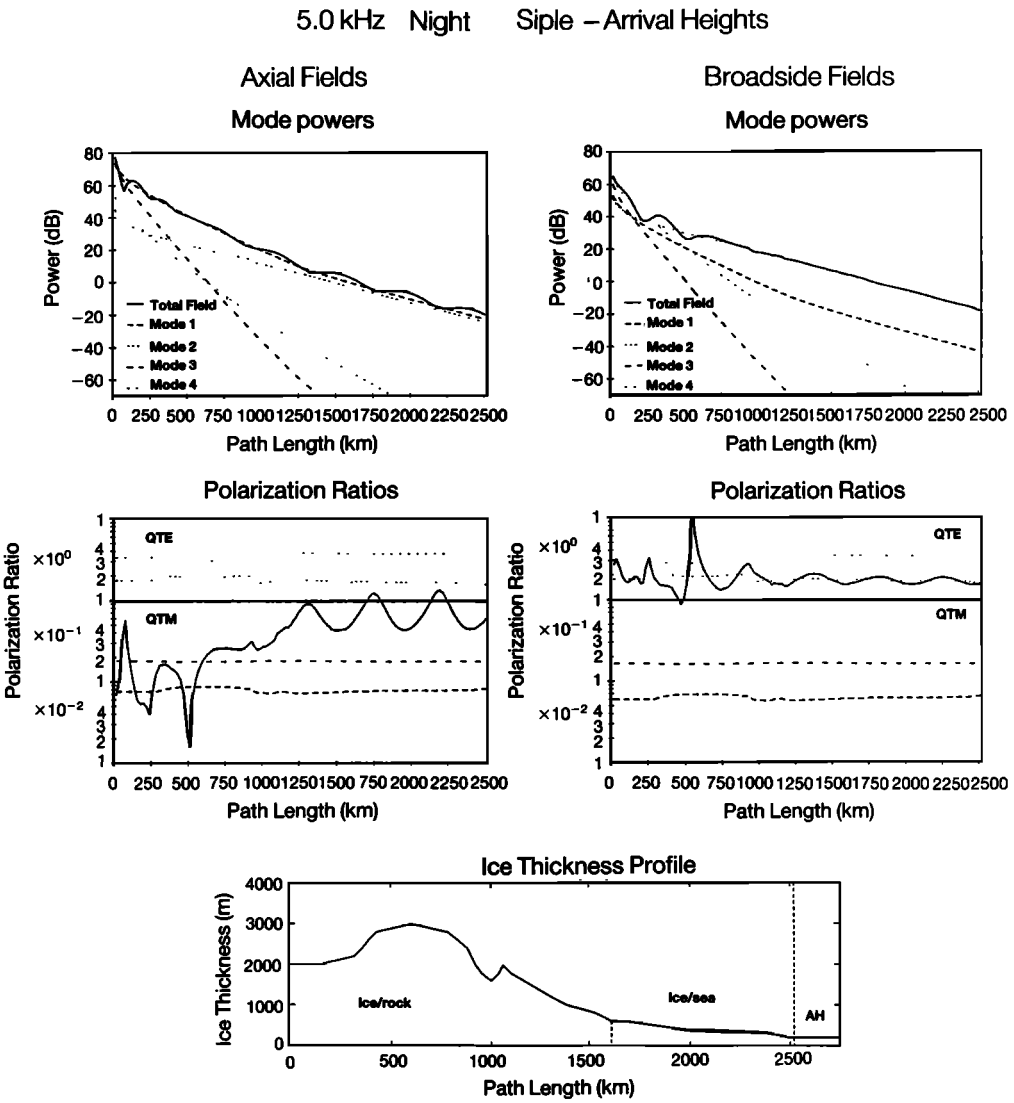

Fig. 5. Mode powers and polarization ratios for a 5-kHz signal propagating between Siple and Arrival Heights under a nighttime ionosphere (Table 3). Fields for signals excited broadside (right-hand panels) and axially (left-hand panels) from the transmitting dipole are given. The bottom center panel shows the variation in the ice thickness profile along the great circle path, plotted by joining the midpoints of the individual sections of constant ice thickness.

attenuation. Therefore the axial signal (Figure 6, left-hand panels) remains dominated by the most strongly excited mode, mode 1, and retains a QTM polarization ratio of less than unity. The broadside signal received at Halley retains its initially excited, mixed polarization, form. The two higher-order modes, 3 and 4, undergo higher attenuation and become insignificant. The difference in total broadside and axial signal strengths received at Halley will therefore be close to 15 dB, equal to the difference in excitation of mode 2 at $\phi = 0°$ (−40 dB), and mode 1 at $\phi = \pm 90°$ (−25 dB), with an extra positive or negative contribution from mode 2 on the broadside signal.

The modeled variations along the path to Faraday were similar to those illustrated for the Halley GC path in Figure 6, though the QTM mode 1 showed a slightly higher overall attenuation because of the differences in the detail of the topology of the ground, and because of the use of a mid-latitude ionospheric model. Thus mode 1 makes a slightly weaker contribution to the

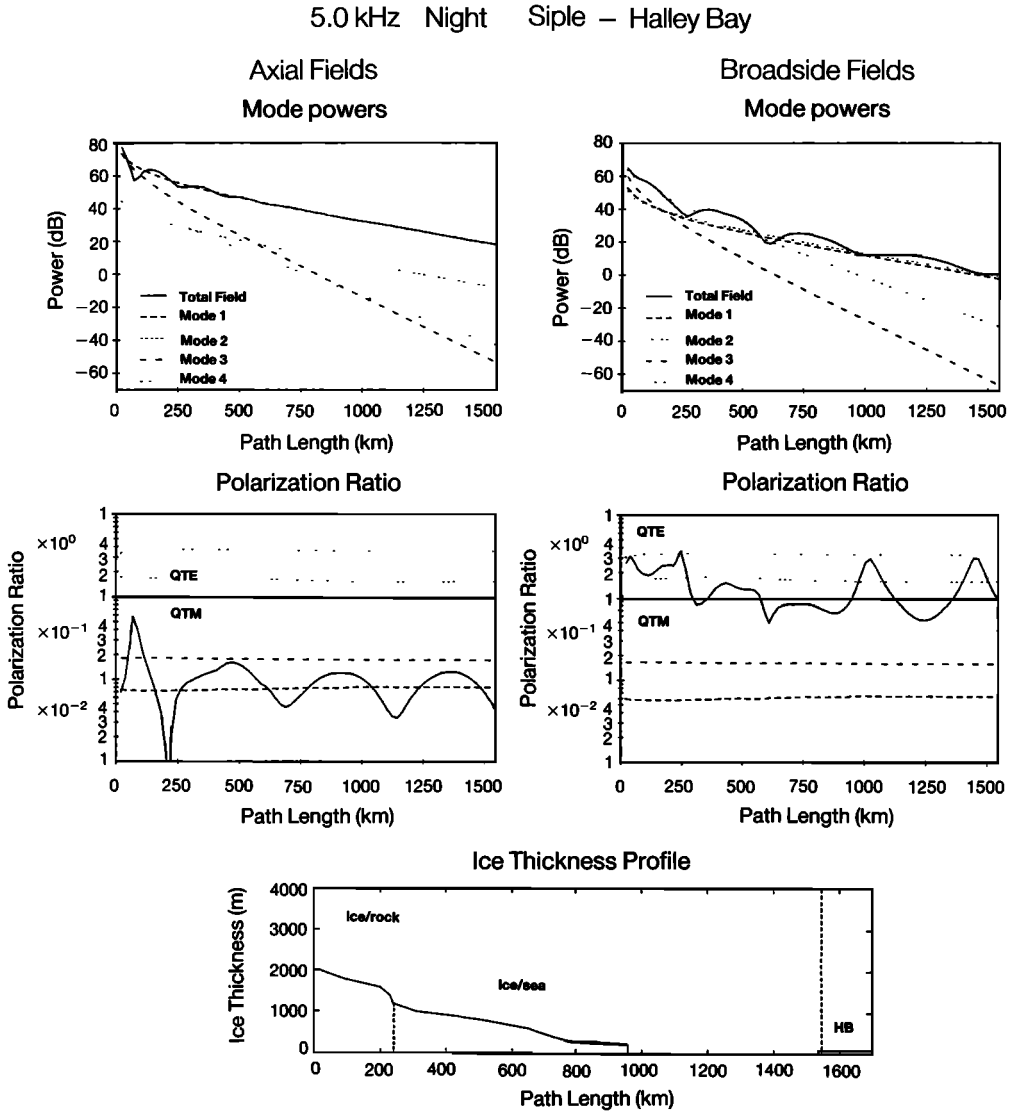

Fig. 6. Mode powers and polarization ratios for a 5-kHz signal propagating between Siple and Halley under a nighttime ionosphere (Table 3). Fields for signals excited broadside (right-hand panels) and axially (left-hand panels) from the transmitting dipole are given. The bottom center panel shows the variation in the ice thickness profile along the great circle path, plotted as for Figure 5.

broadside signal and remains dominant (but less so) on the axial signal. The GC path from Siple to South Pole, though entirely over ice, crosses the mountains of the Vinson Massif, where the ice thins to less than 500 m. Also, as mentioned above, the single loop antenna used to receive the signals at South Pole is aligned so that it preferentially received QTM polarized modes from Siple. The model then calculated that the signal received at South Pole could be represented as lying somewhere between the two extremes of Figures 5 and 6, with the axial signal still dominated by mode 1 (~10 dB stronger than mode 2), and modes 1 and 2 of almost equal strengths in the broadside signal.

Unfortunately, the model could not find solutions for the mode equation (equation (8)) for signals with frequencies $\lesssim$3 kHz. At these frequencies the mode angles change rapidly with small variations in waveguide and signal parameters, and the iterative method used to solve (8) could not be forced to converge. It is possible that a more accurate ionospheric model or different

iterative method may have allowed solution of the mode equation in such cases. The detailed modeling work presented in this paper is therefore restricted to the 5-kHz signals.

WAVEGUIDE EXPERIMENT RESULTS: DISCUSSION

Variations in received signal power

Figure 7 presents the variations in recorded signal power plotted against Siple transmitter antenna orientation, for June 27, 1986. The equivalent results from the computer model (dashed lines) are provided for comparison. The recorded data power values are calculated with respect to 1 pT; the modeled values have had their reference levels altered to facilitate comparison (HB by −10 dB, FA by −15 dB, SP by −20 dB, and AH by −5 dB). The recorded data showed some day-to-day variation (~5 dB for the 5-kHz nighttime transmissions) but the essential feature of Figure 7, a minimum in power for $\phi = 0°$ (broadside excitation) which decreased from Halley (~20 dB) to Arrival Heights (no minimum), was repeatable.

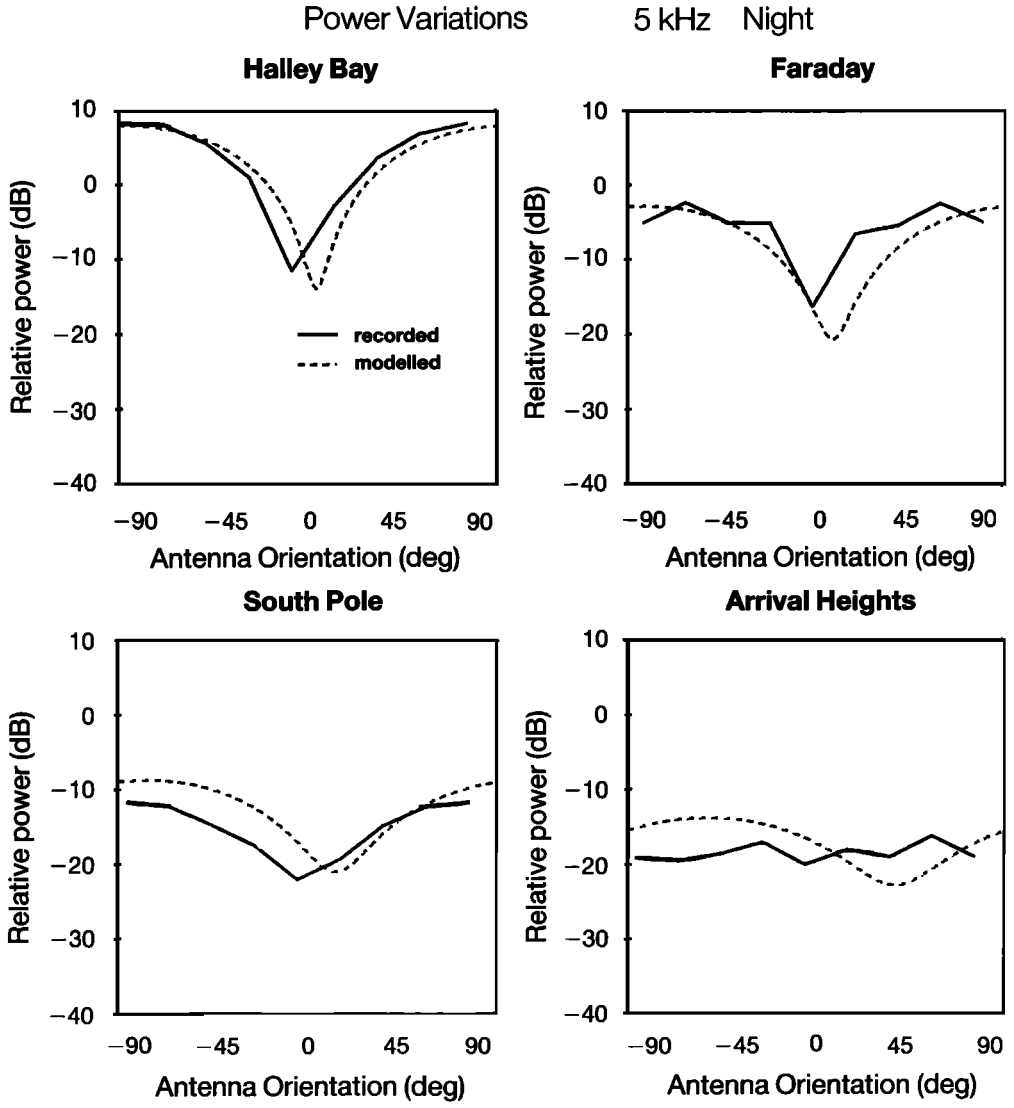

Fig. 7. Recorded and modeled variations in received signal power for different orientations of the transmitting dipole with respect to the great circle propagation paths. The signal frequency is 5 kHz, and it is traveling under a nighttime ionosphere (Table 3); the recorded data are for June 27, 1986.

From the discussions in the previous section, we know that the broadside minimum is initially caused by the less efficient excitation of the waveguide at this antenna orientation. The size of the minimum decreases when the path crosses over large sections of thick ice sheet, as the QTM mode (mode 1), excited most strongly for $\phi = 0°$, undergoes more attenuation than (QTE) mode 2. At Arrival Heights the influence of mode 1 in the broadside signal is minimal, and modes 1 and 2 are of equal strength in the axial signal. Thus the variation of power with ϕ at Arrival Heights more closely resembles the antenna radiation pattern of mode 2 than that of mode 1, hence the absence of a broadside minimum.

The modeled results recreate the magnitudes of the broadside minima remarkably well, confirming that the excitation functions and attenuation rates of modes 1 and 2, relative to each other, are accurate. The necessary alterations in power reference levels of the modeled results reflect some uncertainties in factors affecting absolute excitation functions (such as the height of the transmitting dipole above the ice sheet) and possibly some inaccuracies introduced as a result of the simple ground and ionospheric models.

Note that the positions of the maxima and minima in the recorded data and modeled results do not exactly correspond. This is largely because the computer model generated signal values for 2° antenna steps, whereas the actual antenna positions simulated during the waveguide probing experiment were at 22.5° intervals. There was therefore always a discrepancy, of up to 11.25°, between the antenna positions which were closest to broadside on ($\phi = 0°$) and end on ($\phi = \pm 90°$) and the orientations corresponding exactly to these directions. Further sources of error, possibly leading to slight inaccuracy in the simulated antenna positions, could be a lack of exact orthogonality in the two dipoles and small differences in the power applied to the two antenna-elements.

The 3-kHz transmissions (only Faraday and Halley data available) showed smaller, 5–10 dB, minima, and variations in absolute power levels from day to day were larger (~8 dB). It is likely that the radiation pattern of the dipole at 3 kHz is similar to that at 5 kHz, so it would appear that mode 1 (QTM), dominant at $\phi = \pm 90°$, is more strongly affected than mode 2 (QTE) by the decrease in frequency.

Other workers have noted that the propagation of signals with frequencies at the low end (2–3 kHz) of the VLF range shows a greater variability than that of higher frequency signals (~7.5 kHz) [*Carpenter et al.*, 1988]. This high sensitivity (see also the section above on modeled propagation characteristics) is probably a consequence of a large peak in the attenuation rate for the lowest-order QTM mode, which lies between 2 kHz and 3 kHz [*Barr*, 1971*a*]. Any variation in the ionospheric conditions which results in a slight change of the frequency of this attenuation peak will then have a significant effect on the propagation parameters of signals with frequencies close to this peak. QTE modes do not show an attenuation peak at these frequencies, and so signals dominated by QTE modes will not exhibit such sensitivity.

Because of the more disturbed magnetic conditions that were prevalent during the September transmissions, recorded data were separated into those occurring on days when $Kp \leq 2$, and those recorded when $Kp > 2$. None of the transmissions at 3 kHz (in September) could be identified on the recordings made at any of the receiving stations, presumably, a result of high daytime attenuation reducing the signal strength to beneath that of the noise. Figure 8 presents the power variations at Halley in the 5-kHz signals. The axial signal on the disturbed days can be seen to be ~10 dB weaker than on the quiet days, a result of higher attenuation and/or weaker excitation of mode 1 (dominant at this orientation). A similar effect was obtained with the model by further reducing the daytime ionospheric reflection height of the "disturbed" ionosphere from 82 km to 80 km. It would appear that, at this reflection height and signal frequency, some kind of waveguide cutoff has been reached for mode 1.

In Table 4 the average signal powers recorded at the four stations are given in decibels with respect to 1 pT, for signals excited broadside to, and along the axis of, the transmitting dipole. The dominant modes of each signal, as determined by the computer model, are indicated in parentheses. From the values of this table, it is possible to make some estimates for the attenuation

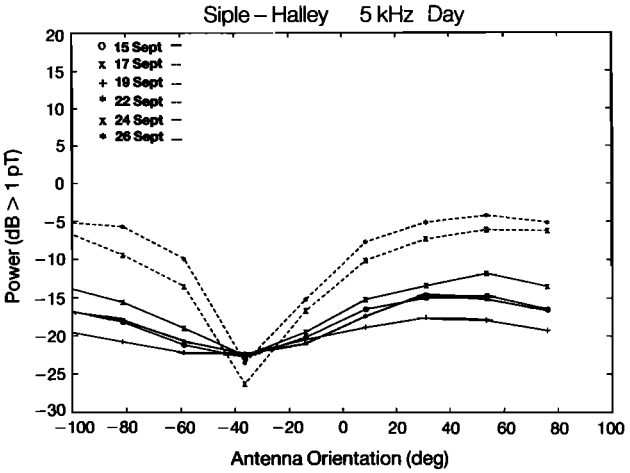

Fig. 8. The variation in received power with antenna orientation at Halley, for a 5-kHz signal under a daytime ionosphere. Results for 6 days are given; the variations represented by dashed lines were recorded on days when $Kp \leq 2$; solid lines represent data for days when $Kp > 2$.

TABLE 4. Average Recorded Signal Strengths, dB > 1 pT

	5-kHz Night		5-kHz Day		3-kHz Night	
	axial	broadside	axial	broadside	axial	broadside
HB	6.1 (1)	−12.8 (1 & 2)	−5.6, −16.5 (1)	−24.9, −22.6 (1 & 2)	−9.8 (1 ?)	−20.4 (1 & 2 ?)
FA	−4.0 (1)	−15.1 (1 & 2)	−9.7, −13.7 (1)	−26.6, −28.1 (1 & 2)	−15.1 (1 ?)	−20.2 (1 & 2 ?)
SP	−11.5 (1)	−22.0 (1 & 2)	...	...	...	...
AH	−22.0 (2)	−22.0 (2)	...	...	...	...

Dominant modes at receiver in parentheses. For 5-kHz day, the two values are for $Kp \leq 2$ and $Kp > 2$ respectively.

rates of the dominant modes, for the first time independent of excitation effects, and dependent on the model only to the extent of the determination of the dominant mode(s). To enable us to make such estimates, we must first make the following generalized comparisons between the individual great circle propagation paths from Siple (refer to Figures 1, 5 and 6).

1. The essential difference between the SI–HB and the SI–AH paths is an extra ~1000 km of thick (>2 km) ice on the SI–AH path.
2. The main difference between the SI–AH and SI–SP paths is an extra ~1000 km over the Ross Ice Shelf (~300-m thick).
3. The difference between the SI–HB and SI–SP paths, is over the latter 1000 km of both paths, where the HB path is half over sea and half over floating ice shelf, and the SP path is over deep (> 1.5-km) ice.

Obviously, these are crude generalizations, and they take no account of a geographically varying ionosphere. Any attenuation rates that are derived must therefore be treated only as approximate values. The above approximations include a maximum error of ±200 m in ice thickness, and so (referring to Figure 4) we have introduced errors (for mode 1, 5-kHz nighttime ionosphere) of ~ ±6 dB Mm^{-1} for propagation over thick (1.5–2.0 km) ice, and of ~ ±2 dB Mm^{-1} for propagation over sea and shelf ice (thickness < 400m). We already have an error of ±2.5 dB on recorded signal strengths, (for paths ~1500 km long), so we now have total estimated maximum errors of ~ ±8 dB Mm^{-1} for propagation over $\gtrsim$ 1.5-km ice, and ± 4 dB Mm^{-1} for propagation over ice shelf and sea (still for mode 1).

From Table 4, we can see that there is a ~28 dB difference between the signal strengths of the axially excited signals at HB and AH. This indicates that mode 1 has undergone an attenuation of at least 28 dB over the extra 1000 km of thick (>2 km) ice. Thus we have an attenuation rate over ≥2-km thick ice, for (QTM) mode 1, of a 5-kHz signal under a nighttime high-latitude ionosphere, of 28 ± 8 dB Mm^{-1}.

Second, the ~10-dB difference between the strengths of the axially excited signals at SP and AH can be attributed to the extra 1000 km over the Ross Ice Shelf on the SI–AH path. This gives an attenuation rate over ~300-m thick floating ice shelf of ~10 ± 4 dB Mm^{-1}.

Finally, a comparison of the SP and HB axial signal strengths in Table 4 indicates an extra attenuation of ~17.5 dB over the South Pole GC path. From the above, this represents an extra attenuation of ~17.5 dB Mm^{-1} for mode 1 over the deep (>2 km) ice of the latter (1000 km) part of the SI–SP path with respect to the attenuation rate over the sea (and shelf ice) of the SI–HB path. Given that modeling work indicated that the thickness of an ice layer must be greater than ~500 m before it has any significant effect, this value would appear to be consistent with the approximate attenuation rates derived above for >2-km thick ice (28 ± 8 dB Mm^{-1}) and sea/shelf ice (~10 ± 4 dB Mm^{-1}).

It is not possible to derive similar values for (QTE) mode 2 because this mode is only dominant on the signal excited broadside to the dipole at Arrival Heights. However, the computer model has been shown above to provide accurate values for mode 2 (QTE) attenuation rates relative to mode 1 (QTM) attenuation rates, with mode 2 showing 10–15 dB Mm^{-1} less attenuation (Figure 4) for ice thicknesses from 1.5 km to greater than ~2.5 km. Over sea and ice shelves the attenuation rates of the two modes were seen to be approximately equal (Figures 5 and 6).

The great circle path from Siple to Faraday covers a ground surface of too great a variability (including many short length sections over sea, ice shelf, and small islands) to allow similar calculations to be made.

Arrival azimuth, ellipticity and elevation measurements

It has been established that signals which are QTE polarized (i.e., with their electric vector in the y direction) will display apparent errors in azimuth and elevation measurements [*Strangeways*, 1980; *Tsuruda and Ikeda*, 1979; *Tkalcevic*, 1983] and that the ellipticity data indicate whether or not the received signal is linearly polarized. We can therefore use the recorded variations in these data to test our estimates of the mode structure and to establish further the accuracy of the computer model. The recorded variations (solid line) of

Figure 9 in ellipticity, azimuth and elevation (at Halley), were typical of the variations recorded during each sequence of transmissions. Although the sizes of the peaks in azimuth and elevation and the extent of the central deviation from zero in the ellipticity data varied from day to day, the senses and patterns of variation were repeatable. This was true for the 5-kHz daytime transmissions, the 3-kHz nighttime transmissions, and the goniometer-bearing measurements at Halley and Faraday. On a number of occasions the recorded azimuth data also showed a "wrap around" feature, in which the azimuth error (as plotted in Figure 9) would swing

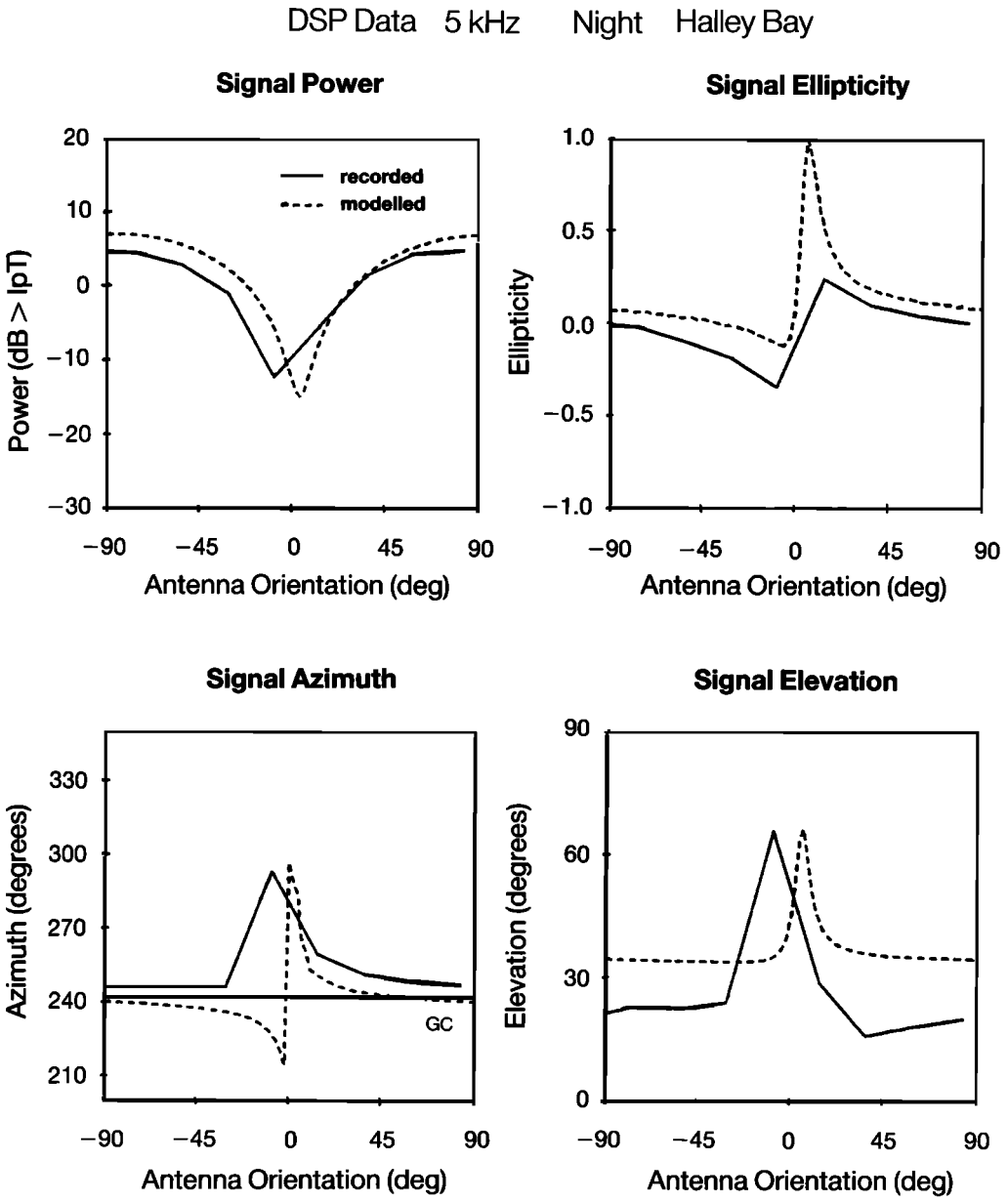

Fig. 9. Variations in recorded and modeled DSP signal characteristics with transmitting antenna orientation, for a 5 kHz signal received at Halley after propagating under a nighttime ionosphere. The horizontal line marked GC indicates the true bearing of the great circle propagation path. Recorded data are from July 25, 1986.

negative before exhibiting the large positive peak and returning to zero. The 22.5° interval between different transmitting antenna positions meant that any such variations, at positions close to broadside excitation, could not be fully investigated, and so the extent or repeatability of this effect could not be reliably established.

The apparent errors in the elevation and azimuth measurements at Halley and Faraday (azimuth only) occur when the signal is of mixed polarization (i.e., when $\phi \approx 0°$). These errors become small when the antenna moves end on, and the received signal becomes dominated by (QTM) mode 1. The ellipticity data confirm this analysis, with values close to 0 (indicating linear polarization) at $\phi \approx \pm 90°$ and an increasing departure from linearity as ϕ moves to 0°. The computer-modeled results can be seen to represent the sense of these variations well and lie well within the day-to-day variation of these parameters. Note that the modeled ellipticity and azimuth exhibit a "wrap around" effect (see above), caused by a reversal in the phase of the dominant excitation coefficients as ϕ moves from positive to negative (equations (13)–(14)).

The modeled values for azimuth, elevation and ellipticity were found to be particularly sensitive to changes in the ionospheric model, a consequence of the oscillations in p_{total} for mixed polarization signals (Figures 5 and 6). This sensitivity was also apparent in the recorded data (particularly the nighttime data) in that large variations occurred in the peak values for azimuth ($\delta\psi \sim 70°$), elevation ($\delta\beta \sim 50°$), and ellipticity ($\delta\eta \sim 0.3$)

Note that these conclusions are slightly different from the findings of *Tkalcevic* [1983]. Here we have found that the signals resulting from excitation broadside to the dipole have a mixed polarization rather than being purely horizontally polarized (with respect to the electric vector, i.e., QTE), as reported by *Tkalcevic* [1983].

Third harmonics

Weak third harmonics were recorded at Halley on the 3-kHz signal when the transmitting dipole was at the three orientations closest to $\phi = 0°$. No third harmonics of the 5-kHz signal were recorded at Halley, though special recordings with a 15-kHz bandwidth were made. The lack of detection of strong third harmonic signals at Halley is not well understood. It is possible that the reception in 1983, at Halley, of large-amplitude third harmonics of a 2.5-kHz fundamental [*Carpenter et al.*, 1988] was a consequence of the lower frequencies involved, resulting in differences in radiation efficiency and propagation properties. In that year the longer, 21.4-km, dipole transmitting antenna was in use, which had a half wave resonant frequency close to that of the 2.5-kHz fundamental.

At Faraday, South Pole and Arrival Heights, any third harmonic signals were below the noise levels. This was not unexpected, taking into consideration the weakness of these signals at Halley and the lower signal strengths of the fundamentals at the other three stations.

Circularly polarized signals

The circularly polarized transmission format was designed primarily to achieve efficient excitation of whistler modes into the magnetosphere. However, this format also excited subionospheric signals, and these were recorded at all four receiving stations.

At Faraday and Halley, the difference between the received powers of the two circularly polarized transmissions was of varying sign, and on average $\leq$ 2 dB, not significant when compared to the variations of the other signals of the transmission sequence (10–20 dB). However, at South Pole and Arrival Heights, the two circularly polarized transmissions were received with consistent and large differences in signal strength. At South Pole the right-hand circularly (RHC) polarized signal was consistently 7–8 dB stronger than the left-hand circularly (LHC) polarized signal, whereas at Arrival Heights the LHC signal was consistently 8–13 dB stronger than the RHC signal. The signals initially launched into the waveguide from these transmissions would not be circularly polarized but would cycle between an axially excited linearly polarized (QTM) signal and a mixed polarized signal excited broadside to the dipole. The exact polarization at the two limits of antenna orientation will vary as the signal propagates over the ice. However, there is no apparent reason why these two signals should display such obviously different propagation characteristics along the paths to South Pole and Arrival Heights.

The circularly polarized signals received at Halley exhibited low azimuth and elevation errors and displayed an ellipticity of $\leq$ 0.2, indicating that at Halley these signals were mostly linearly polarized.

CONCLUSIONS

The data from the waveguide probing experiment, and the accompanying analysis with the aid of the computer model, have provided important information on the propagation characteristics of VLF signals (3 kHz $\leq f \leq$ 5 kHz) over the Antarctic. The comparison of model results and recorded data has verified the accuracy of a simple model for the Earth-ionosphere waveguide.

It may also be noted that the simulation of the rotating dipole, by the use of the two stationary orthogonal dipoles, was achieved with almost total success by the operators at Siple.

It has been established that a simple waveguide propagation model, which included four modes, has represented VLF propagation on the great circle paths from Siple to Faraday, Halley, Arrival Heights and South Pole with a fair degree of accuracy. The computer model predicted an asymmetric radiation pattern from the Siple dipole, with QTM modes being excited most strongly along the axis of the dipole. Modeled and recorded data were used together to establish approximate nighttime attenuation rates for the two lowest-order modes of a 5-kHz signal. These attenuation rates were; for mode 1, 10 ± 4 dB Mm^{-1} over < 300-m shelf ice and sea and 28 ± 8 dB Mm^{-1} over > 1.5-km-thick ice, and for mode 2, 10 ± 4 dB Mm^{-1} over < 300-m shelf ice and sea and 13 ± 8 dB Mm^{-1} over > 1.5-km-thick ice. These results give higher attenuation rates than may have been expected from previously derived daytime rates for mode 1 [*Field et al.*, 1972; *Dowden and Holzworth*, 1988] and provide the first experimental confirmation of the low attenuation of QTE modes over thick ice.

Other variations in the recorded data have indicated that the attenuation rates of the QTM modes are more sensitive to a reduction in the signal frequency than those of QTE modes and that the daytime Antarctic waveguide appears to exhibit some form of cutoff for reflection heights ~80 km for the lowest-order mode of a 5-kHz signal.

These findings have many direct applications to all studies involving subionospheric VLF propagation over the Antarctic, specifically with regard to investigations which are sensitive to the polarization of the incoming signal (e.g., direction finding on whistlers). The results may be particularly relevant to the interpretation of both natural and man-made VLF signals received at a network of Automatic Geophysical Observatories (AGOs), which it has been proposed should be deployed over the Antarctic continent. A possible engineering solution to the problem of timekeeping on AGOs, that is, using Omega, also relies on the characteristics of VLF propagation over the Antarctic interior.

The modeling work has also suggested that, by careful selection of signal frequency and antenna orientation, signals with known polarization and propagation characteristics may be excited and can then be used to probe specific regions of interest within the waveguide. This application could be of particular use in studies of the effect of wave-induced burst precipitation of energetic electrons on subionospheric VLF signals (the Trimpi effect), as described in a companion paper [*Cotton and Smith*, 1991].

Acknowledgments. We are grateful to the field personnel at Siple, South Pole, Arrival Heights, Halley and Faraday for the operation of this experiment. The VLF project at Halley was supported by the Natural Environmental Research Council. The work at Stanford was sponsored by the Division of Polar Programs of the National Science Foundation under grants DPP 86-13783, 87-20167 and 89-18326. The acquisition of data at Arrival Heights was supported in part by the U.S. Office of Naval Research under grant N00014-90-J-1080. PDC acknowledges financial support in the form of a Science and Engineering Research Council research studentship.

REFERENCES

Barr, R., The propagation of ELF and VLF radio waves beneath an inhomogeneous anisotropic ionosphere, *J. Atmos. Terr. Phys., 33*, 343–353, 1971*a*.

Barr, R., The effect of the Earth's magnetic field on the propagation of ELF and VLF radio waves, *J. Atmos. Terr. Phys., 33*, 1577–1583, 1971*b*.

Barr, R., The nocturnal *D*-region as seen by VLF radio waves, *J. Atmos. Terr. Phys., 44*, 407–413, 1982.

Barr, R., The diffraction of VLF radio waves by the Antarctic ice cap, *J. Atmos. Terr. Phys., 49*, 1–5, 1987.

Bullough, K., and J. L. Sagredo, VLF goniometer observations at Halley Bay, Antarctica, 1, The equipment and measurement of signal bearing, *Planet. Space Sci., 21*, 899–912, 1973.

Carpenter, D. L., U. S. Inan, E. W. Paschal, and A. J. Smith, A new VLF method for studying burst precipitation near the plasmapause, *J. Geophys. Res., 90*, 4383–4388, 1985.

Carpenter, D. L., T. F. Bell, and A. J. Smith, The Siple VLF transmitter as a multi-frequency probe of the Earth-ionosphere waveguide, *J. Atmos. Terr. Phys., 50*, 105–115, 1988.

Cotton, P. D., and A. J. Smith, The signature of burst particle precipitation on VLF signals propagating in the Antarctic earth-ionosphere waveguide, *J. Geophys. Res., 96*, 19,375–19387, 1991.

Dowden, R. L., and R. H. Holzworth, Sub-ionospheric propagation at 5 kHz over and in the vicinity of Antarctica, *J. Geomagn. Geoelectr., 40*, 1437–1444, 1988.

Drewry, D. J., Antarctic ice sheet thickness and volume, *Sheet 4, Antarctica: Glaciological and Geophysical Folio*, Scott Polar Research Institute, Cambridge, England, 1983.

Field, E. C., C. Greifinger, and K. Schwartz, Transpolar propagation of long radio waves, *J. Geophys. Res., 77*, 1264–1278, 1972.

Galejs, J., *Terrestrial Propagation of Long Electromagnetic Waves*, Pergamon, Elmsford, New York, 1972.

Harth, W., Theory of low frequency wave propagation, in *CRC Handbook of Atmospherics*, edited by H. Volland, CRC Press, Boca Raton, Fla., 1982.

Helliwell, R. A., VLF wave stimulation experiments in the magnetosphere for Siple station, Antarctica, *Rev. Geophys., 26,* 551–578, 1988.

Helliwell, R. A., and J. P. Katsufrakis, Controlled wave-particle interaction experiments, in *Upper Atmospheric Research in Antarctica,* edited by L. J. Lanzerotti and C. G. Park, AGU, Washington D. C., 1978.

Inan, U. S., and D. L. Carpenter, Lightning induced electron precipitation events observed at $L\sim4$ as phase and amplitude perturbations on subionospheric signals, *J. Geophys. Res., 92,* 3293–3303, 1987.

Kelly, F. J., A. J. Martin, S. H. Knowles, E. S. Byrd, M. Andrews, L. DeBlasio, J. Siegel, D. Clamons, N. Sheely, M. Deebel, T. Priddy, L. Quinn, and F. J. Rhoads, Developments in Arctic long-wave propagation theory and experiments, *Radio Sci., 23,* 240–246, 1988.

Kelly, F. J., and E. S. Byrd, The effect of ice temperature on propagation of VLF waves across Greenland, in *Proceedings of the 5th URSI Commission F symposium, Wave Propagation and Remote Sensing, La Londe-les-Maures, France, Sept. 1989,* URSI, Gent, Belgium, 1989.

Kossey, P. A., J. P. Turtle, R. P. Pagliarulo, W. I. Klemetti, and J. E. Rasmussen, VLF reflection properties of the normal and disturbed polar ionosphere in northern Greenland, *Radio Sci., 18,* 907–916, 1983.

Morfitt, D. G., and C. H. Shellman, 'MODESRCH', an improved computer program for obtaining ELF/VLF/LF mode constants in an Earth-ionosphere waveguide, *Interim Rep. 77T,* Nav. Electron. Lab. Cent., San Diego, Calif., 1976.

Pappert, R. A., Effects of elevation and ground conductivity on horizontal dipole excitation of the earth-ionosphere waveguide, *Radio Sci., 5,* 579-590, 1970.

Pappert, R. A. and J. A. Ferguson, VLF/LF mode conversion model calculations for air to air transmissions in the Earth-ionosphere waveguide, *Radio Sci., 21,* 551–558, 1986.

Pappert, R. A. and F. P. Snyder, Some results of a mode conversion program for VLF, *Radio Sci., 7,* 913–923, 1972.

Peden, I. C., G. E. Webber and A. S. Chandler, Complex permittivity of the Antarctic ice sheet in the VLF band, *Radio Sci., 7,* 645–650, 1972.

Raghuram, R., R. L. Smith and T. F. Bell, VLF Antarctic antenna: impedance and efficiency, *IEEE Trans. Antennas Propag., AP-22,* 334–338, 1974.

Smith, A. J., and K. H. Yearby, AVDAS— A microprocessor-based VLF signal acquisition, processing and spectral analysis facility for Antarctica, *Br. Antarct. Surv. Bull., 75,* 1–15, 1987.

Strangeways, H. J., Systematic errors in VLF direction-finding of whistler ducts, 1, *J. Atmos. Terr. Phys., 42,* 995–1008, 1980.

Tkalcevic, S., Very low frequency signals (2–10 kHz) received at Palmer station, Antarctica, from the 21.4 km dipole antenna at Siple station, 1400 km distant, *J. Atmos. Terr. Phys., 45,* 353–367, 1983.

Tolstoy, A., T. J. Rosenberg, U. S. Inan, and D. L. Carpenter, Model predictions of subionospheric VLF signal perturbations resulting from localised electron precipitation induced ionization enhancement regions, *J. Geophys. Res., 91,* 3473–3482, 1986.

Tsuruda, K. and M. Ikeda, Comparison of three different types of VLF direction finding techniques, *J. Geophys. Res., 84,* 5325–5332, 1979.

Wait, J. R., *Electromagnetic Waves in Stratified Media,* Pergamon, Elmsford, New York, 1962.

Wait, J. R., and L. B. Perry, Calculations of ionospheric reflection coefficients at very low frequencies, *J. Geophys. Res., 62,* 43–56, 1957.

Watson, G. N., *A Treatise on the Theory of Bessel Functions,* Cambridge University Press, New York, 1922.

Webber, G. E., and I. C. Peden, VLF fields of a horizontal dipole below the polar anisotropic ionosphere, *IEEE Trans. Antennas Propag., AP-19,* 523–529, 1971.

Westerlund, S., and F. H. Reder, VLF radio signals propagating over the Greenland ice sheet, *J. Atmos. Terr. Phys., 35,* 1475–1491, 1973.

D. L. Carpenter, W. L. Poulsen, and T. G. Wolf, Space Telecommunications and Radioscience Laboratory, Stanford University, Stanford, CA 94305.

P. D. Cotton, James Rennell Centre for Ocean Circulation, Gamma House, Chilworth Research Centre, Chilworth, Southampton SO1 7NS, England.

A. J Smith, British Antarctic Survey, High Cross, Madingley Road, Cambridge CB3 0ET, England.